Structure and dynamics of water adsorbed on the lignite surface: Molecular dynamics simulation

Xiaofang You [1], Meng He [1], Xiaoqiang Cao [1], Xianjun Lyu [1], Lin Li [1]

[1] College of Chemical and Environmental Engineering, Shandong University of Science and Technology, Qingdao 266590, China.

Corresponding author: lilin_1983123@sdust.edu.cn (Lin Li)

Abstract: The effects of oxygen-containing functional groups on the structure and dynamic properties of water molecules near a lignite surface were investigated through molecular dynamics (MD) simulations. Because of its complex composition and structure, a graphite surface containing hydroxyl, carboxyl, and carbonyl groups was used to represent the lignite surface model. According to X-ray photoelectron spectroscopic (XPS) results, the composing proportion of hydroxyl, carbonyl and carboxyl is 21:13:6. The density profiles of oxygen and hydrogen atoms indicate that the brown coal surface characteristics influence the structural and dynamic properties of water molecules. The interfacial water is much more ordered than bulk water. The results of the radial distribution functions, mean square displacements, and local self-diffusion coefficients for the water molecules in the vicinity of three oxygen-containing functional groups confirmed that carboxyl groups are the preferential adsorption sites.

3. Introduction

Low rank coal (LRC) is very abundant on earth and is composed of brown coal and subbituminous coal (Osman et al., 2011; Zhang et al., 2016). However, the high moisture content in LRC restricts its large-scale utilization (Willson et al., 1997). It has been found that the large amount of oxygen-containing functional groups on the surface of LRC determines its high moisture content (Zhou et al., 2016; Tian et al., 2016a, 2016b; You et al., 2017). Oxygen-containing functional groups in LRC can be mainly categorized into carbonyl, carboxyl, and hydroxyl and generally exhibit strong hydrophilicity (Bhattacharyya, 1971). Intramolecular and noncovalent intermolecular interactions between LRC and water, such as charge transfer, van der Waals, and hydrogen bonding, have been revealed (Larsen and Baskar, 1987; Quinga and Larsen, 1987; Miyake and Stock, 1988; Liu et al., 1993). It has been reported that hydrogen bonding is the dominant effect, that different oxygen functional groups have different hydrogen bonding abilities, and that the carboxyl group is the preferential adsorption site during hydration processes (Allardice and Evans, 1971; Norinaga et al., 1998; Nishino, 2001).

A large number of investigations on the interaction between LRC and water, mainly employing experimental techniques such as proton nuclear magnetic resonance (^{1}H NMR), Fourier transform infrared (FTIR) spectroscopy, and differential scanning calorimetry (DSC), have been performed. However, a complete microscopic understanding of the LRC hydration process is lacking. Molecular dynamics (MD) is an effective tool to get further knowledge on this kind of processes. Zhang (2011) investigated the structure and dynamics of a lignite/water system, with a moisture content ranging from 0 to 60%, using MD simulations. Wu et al. (2016) theoretically studied noncovalent interactions between LRC and water. Vu et al. (2002) investigated the interactions between a lignite model, based on lignin, and water via MD.

So far, there have been some experimental studies on the interaction between LRC and water; however, little research on this topic has been performed using MD simulations because of the structural complexity and diversity of lignite. A macromolecular coal model involving several unimolecular coal models has been employed by Wiser (Zhang et al., 2015), Hatcher (Lyu et al., 2018), and Wender (Zhang et al., 2017). However, the surface characteristics of this macromolecular coal model make it not suitable for investigating LRC-water interactions, as will be verified in this paper. A common strategy to obtain surfaces with particular properties is to attach characteristic functional groups to solid substrates (Argyris et al., 2008; Argyris et al., 2009; Tummala et al., 2011). Adopting this surface reconstruction method, precise solid surface features can be systematically obtained. Although a surface model constructed following that strategy represents an approximation to the real solid surface structure, it is a rational model to purely investigate the properties of the lignite surface.

Because the surface of graphene oxide (GO) is similar to that of coal, we built a graphene oxide (GO) surface model with different degrees of oxidation (Shih et al., 2012). A graphite surface incorporating oxygen-containing functional groups was employed to model the lignite surface. X-ray photoelectron spectroscopic (XPS) is a powerful tool to detect surface element and function groups (Gao et al., 2016a, b; Wang et al., 2016; Tian et al., 2017; Li and Gao, 2017; Gao et al., 2017; Gao et al., 2018). Firstly, the proportion of the oxygen-containing functional groups on the surface of the model was estimated based on XPS analyses performed on lignite, an important constituent of the low rank coal, from Zhaotong. Then, the effects of oxygen-containing functional groups on the brown coal surface on the structure and dynamics of interfacial water molecules were examined. The findings of this investigation could possibly provide insights to theoretically describe the interaction between oxygen-containing functional groups and interfacial water at the molecular level.

2. Materials and methods

2.1. Materials

Lignite from Zhaotong, Yunnan Province in China, was selected for this study. The lignite was milled and sieved into 48~75 μm particles. Then, the sample was dried at 100 °C in a vacuum oven for 2 h prior to use. Proximate analysis was performed according to the national standard of China (GB/T212-2008), and the results are shown in Table 1.

Table 1. Proximate analysis of lignite (wt%)

Moisture, ad [1]	*Ash, ad* [1]	*Volatile matter, daf* [2]	*Fixed carbon, daf* [2]
9.10	19.82	62.75	37.25

[1] Air-dry basis; Dry ash-free basis

2.2. XPS measurements

The XPS experiments were performed employing an ESCALAB 250Xi instrument. To eliminate the effect of the mineral matter of the coal on the XPS measurements, the lignite was demineralized using dilute HF and HCl solutions (Mukherjee and Borthakur, 2004; Zhou et al., 2015). Firstly, the sample was treated with a solution containing deionized water, 37% HCl, and 40% HF in a volume ratio of 2:1:1 in a 300 mL beaker for 6 h at 50 °C. Then, it was washed with deionized water until the solution become neutral. In a vacuum oven, the sample was finally dried at 100 °C for 24 h.

2.3. Molecular dynamics simulation methodology

Materials Studio 8.0 was the software used in this research. The COMPASS force field was employed for all simulations. The functional form of this force field is:

$$E_{total} = E_{bond} + E_{angle} + E_{oop} + E_{torsion} + E_{cross} + E_{elect} + E_{lj} \tag{1}$$

where E_{bond} is the bond stretching energy, E_{angle} is the angle bending energy, E_{oop} is the out-of-plane angle energy, $E_{torsion}$ is the bond torsion energy, and E_{cross} is the cross-term interacting energy. E_{lj} and E_{elec} represent the Van der Waals and electrostatic interactions, respectively. A Lennard-Jones potential

is used to describe the Van der Waals interaction. The terms contributing to the total energy can be explicitly written as follows (Lyu et al., 2018; Liu et al., 2013; Yang et al., 2000; Sun et al., 1998; Mcquaid et al., 2004; Bunte and Sun, 2000; He et al., 2018):

$$E_{bond} = \sum_b \left[k_2 \left(b - b_0 \right)^2 + k_3 \left(b - b_0 \right)^3 + k_4 \left(b - b_0 \right)^4 \right] \tag{2}$$

$$E_{angle} = \sum_\theta \left[H_2 \left(\theta - \theta_0 \right)^2 + H_3 \left(\theta - \theta_0 \right)^3 + H_4 \left(\theta - \theta_0 \right)^4 \right] \tag{3}$$

$$E_{torsion} = \sum_\phi \left[V_1 \left[1 - \cos \left(\phi - \phi_0 \right) \right] + V_2 \left[1 - \cos \left(2\phi - \phi_0 \right) \right] + V_3 \left[1 - \cos \left(3\phi - \phi_0 \right) \right] \right] \tag{4}$$

$$E_{oop} = \sum_x K_x x^2 \tag{5}$$

$$
\begin{aligned}
E_{cross} =\ & \sum_{b'} F_{bb'} \left(b - b_0 \right) \left(b' - b_0' \right) + \sum_\theta \sum_{\theta'} \left(\theta - \theta_0 \right) \left(\theta' - \theta_0' \right) \\
& + \sum_b \sum_\theta F_{b\theta'} \left(b - b_0 \right) \left(\theta' - \theta_0' \right) \\
& + \sum_b \sum_\phi F_{b\phi} \left(b - b_0 \right) \left[V_1 \cos \phi + V_2 \cos \left(2\phi \right) + V_3 \cos \left(3\phi \right) \right] \\
& + \sum_{b'} \sum_\phi F_{b'\phi} \left(b' - b_0' \right) \left[V_1 \cos \phi + V_2 \cos \left(2\phi \right) + V_3 \cos \left(3\phi \right) \right] \\
& + \sum_\theta \sum_\phi F_{\theta\phi} \left(\theta - \theta_0 \right) \left[V_1 \cos \phi + V_2 \cos \left(2\phi \right) + V_3 \cos \left(3\phi \right) \right] \\
& + \sum_\theta \sum_{\theta'} \sum_\phi k_{\phi\theta\theta'} \left(\theta - \theta_0 \right) \left(\theta' - \theta_0' \right)
\end{aligned}
\tag{6}
$$

$$E_{elec} = \sum_{i>j} \frac{q_i q_j}{\varepsilon \gamma_{ij}} \tag{7}$$

$$E_{lj} = \sum_{i,j} \varepsilon_{ij} \left[2 \left(\frac{\gamma_{ij}^0}{\gamma_{ij}} \right)^9 - 3 \left(\frac{\gamma_{ij}^0}{\gamma_{ij}} \right)^6 \right] \tag{8}$$

where q_i and q_j are the atomic charges of the atoms i and j, respectively, b are bond lengths, γ_{ij} is the interatomic distance between atoms i and j, χ are out-of-plane angles, ϕ are torsion angles, θ are valence angles, and ε is the dielectric constant. F, k, V, and H represent system-dependent parameters.

The selection of the lignite model is a key point. Two kinds of lignite models were constructed: a macromolecular lignite model and a graphene oxide surface model.

A method similar to that previously reported (Zhang et al., 2015; Zhang et al., 2017; Lyu et al., 2018; You et al., 2018) was used to build a macromolecular model (Fig. 1) containing 80 Wender lignite molecules (Wender, 2006). Five hundred water molecules, placed as shown in Fig. 2 to solvate the solid substrate, were described using the simple point charge/extended (SPC/E) model (Berendsen et al., 1987). The coal-water system was packed into a rectangular simulation cell with dimensions of 30×30×110 Å³ (X×Y×Z).

The modified graphene oxide surface model representing the lignite surface is shown in Fig. 3. The graphite is composed of four graphene sheets with a separation of 3.4 Å between adjacent layers. On the first graphene basal plane, the hydroxyl, carboxyl, and carbonyl groups were randomly grafted to carbon atoms. The composition ratio of these oxygen-containing functional groups was obtained from the XPS results. The water molecules were simulated using the SPC/E model. One lignite model and 500 water molecules were put into a rectangular simulation box with dimensions of 25.6×29.5×70 Å³ (X×Y×Z).

All simulations were performed in the NVT ensemble at 298 K using a Nose thermostat, and the time step was set to 1.0 fs. A van der Waals interaction cutoff of 12.5 Å was employed, and the Ewald

summation method with an accuracy of 10^{-3} kcal/mol was used to account for the long-range electrostatic interactions. The simulation was performed for 1 ns. The final results are based on a production run of 500 ps after an equilibration period.
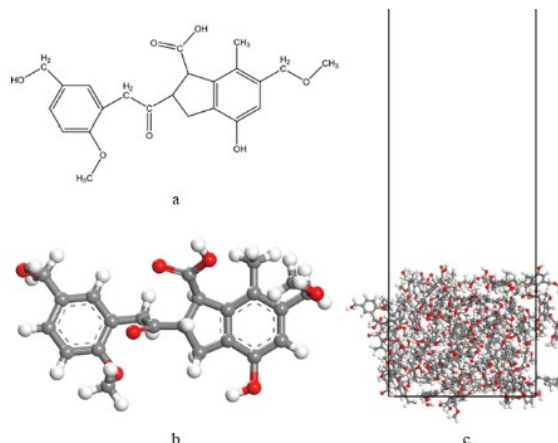

Fig. 1. (a) Molecular model of lignite. (b) The structure of a single lignite model. (c) The structure of 80 optimized lignite model molecules. The fixed atoms in the lignite model are shown in black. The red, grey, and white balls represent O, C, and H, respectively
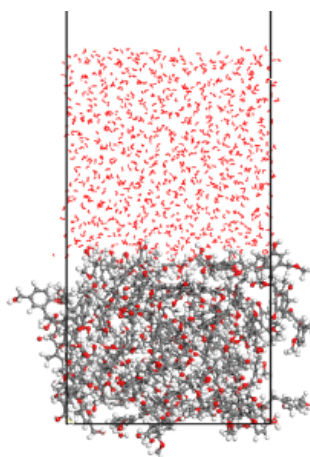
Fig. 2. Side view of the entire simulation box with the water molecules in contact with the lignite surface. The balls colored in red, gray, and white represent O, C, and H, respectively
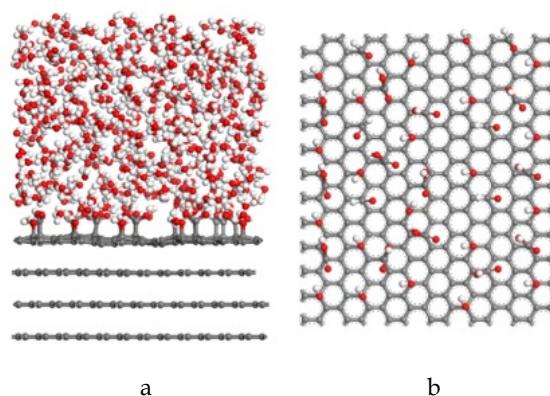

a   b

Fig. 3. Snapshots of the lignite substrates used in our simulations. (a) Side view of the entire simulation box with the water molecules in contact with the lignite surface. (b) Top side view of the lignite model. The balls colored in red, gray, and white represent O, C, and H, respectively

The density profiles were obtained using the following procedure. Relative concentration profiles were obtained directly through Materials Studio 8.0. Firstly, the z axis was divided in equal spaced slabs. Then, the ratio of the total mass on the basis of the relative concentration in the slab to the volume of the slab, which is the density of the slab, was calculated. Finally, the density profile along the z direction was plotted.

The mean square displacement (MSD) is the statistical average of the particle trajectories and can be used to characterize the diffusion of water molecules. The MSD can be expressed as:

$$\text{MSD} = N^{-1} \left\langle \sum_i \left| r_i(t) - r_i(0) \right|^2 \right\rangle \tag{9}$$

where N, $r_i(0)$, and $r_i(t)$ represent the number of atoms in the simulation, the position vector of the atom i at the initial time, and the position vector of the atom i after time t, respectively. The angular brackets mean ensemble average.

The self-diffusion coefficient (D) represents the intensity of atomic mobility, which can be expressed as follows (Tao et al., 2009):

$$D = \frac{1}{6N} \lim_{t \to \infty} \frac{d}{dt} \sum_{i \to j} N \left\langle \left| r_i(t) - r_i(0) \right|^2 \right\rangle \tag{10}$$

The MSD and the self-diffusion coefficient are closely related:

$$D = \lim \left(\frac{MSD}{6t} \right) = \frac{1}{6} K_{MSD} \tag{11}$$

MSD values for the water molecules around carboxyl, carbonyl, and hydroxyl groups were obtained from 500 ps to 750 ps using frames taken every 5 ps. Then, the slopes of the linear fittings to graphs of MSD vs. time were used to calculate the water self-diffusion coefficients around carboxyl, carbonyl, and hydroxyl groups employing equations (10) and (11).

3. Results and discussion

3.1. XPS analysis

In Fig. 4, the XPS wide-scan spectrum of demineralized lignite is presented. The concentrations of surface elements are shown in Table 2. The contents of C 1s and O 1s on the lignite surface are 80.52% and 17.47%, respectively, while those of other elements are relatively low.
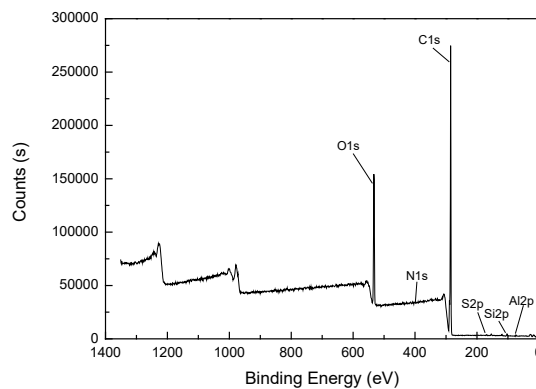

Fig. 4. XPS wide energy spectrum of the lignite surface

A typical curve fitting of the C 1s peak region is shown in Fig. 5. The contents of C-O (hydroxyl or ether), C=O (carbonyl), O=C-O (carboxyl), and C-C/C-H groups were calculated. As shown in Table 3, the content of C-C/C-H, which is the main form of carbon element present on the surface of brown coal, is 79.99% while the contents of C-O, O=C-O, and C=O groups are 10.07%, 6.47%, and 2.83%, respectively.

Because both ether (C–O–C) and hydroxyl (C-OH) groups have carbon-oxygen single bonds, C-O content could not be clearly divided into hydroxyl and ether contributions using XPS. Generally, the content of hydroxyl is much higher than that of ether; therefore, to simplify the lignite model, C-O was considered to be hydroxyl (Pietrzak and Wachowska, 2006; Liu et al., 2017). According to the XPS results, the graphite matrix includes three types of oxygen-containing functional groups (hydroxyl, carbonyl, and carboxyl) in a proportion of 21:13:6, and they cover about 13% of the total surface.

Table 2. Contents of C 1s, O 1s, Si 2p, and Al 2p on the lignite surface

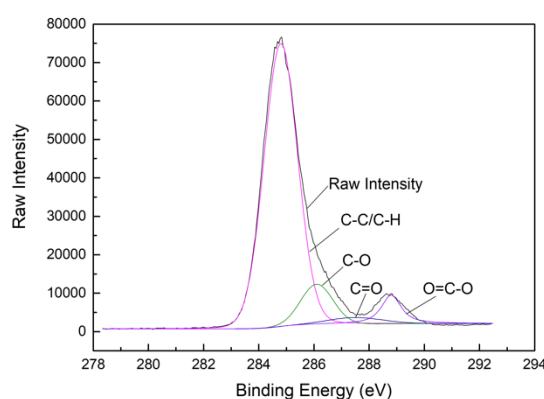| Types	Binding Energy / eV	Contents/%
C_{1s}	284.77	80.52
O_{1s}	532.6	17.47
N_{1s}	399.13	0.49
Si_{2p}	102.83	0.69
Al_{2p}	74.53	0.63
S_{2p}	167.87	0.20

Fig. 5. C 1s peaks for lignite surface

Table 3. The fraction of C on the lignite surface (relative % of C 1s)

Groups	Binding Energy / eV	Contents /%
C-C/C-H	284.80	79.99
O=C-O	288.90	6.47
C=O	287.50	2.83
C-O	286.10	10.70

3.2. MD simulations: selection of the lignite model

The density distributions of the macromolecular lignite model and water molecules along the z axis (normal to the lignite surface) were calculated. As shown in Fig. 6, the top surface of the coal model is located at ~20 Å, and the density of water molecules increases rapidly from ~18.5 Å until an almost constant value of ~0.95 g/cc is obtained at ~27.5 Å. The absence of any remarkable peak in the density profile of water in the vicinity of the coal surface can be attributed to the lack of a hydration layer of water molecules close to the lignite surface. This is an unreasonable result because water molecules are expected to establish strong hydrophilic interactions with the abundant oxygen-containing functional groups on the lignite surface. This apparent contradiction could be caused by the roughness of the lignite model surface. This hypothesis is justified by the apparent density overlap between coal and water molecules, which results from the formation of microscopic valleys, filled by water molecules, on the lignite surface. Therefore, we think that the macromolecular lignite model is not suitable for our study because this model exhibits a rough surface.

The density distribution of water molecules along the z axis is shown in Fig. 7 when the modified graphene oxide surface model is used to represent the lignite surface. In contrast to the macromolecular lignite model, this density distribution displays two obvious peaks indicating the formation of one layer of water molecules near the lignite model surface. This result is in agreement with the strong hydrophilic characteristics of lignite. Hence, the modified graphene oxide surface model was employed in this research.
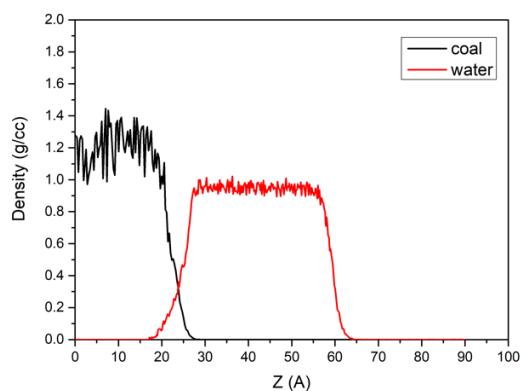
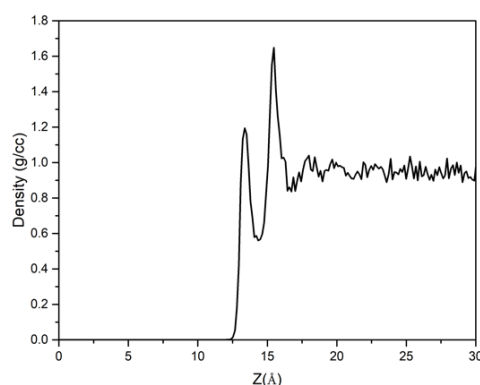Fig. 6 Density distributions of coal and water molecules along the z axis

Fig. 7 Density distribution of water molecules along the z axis using the modified graphene oxide surface model

3.3. MD simulations: structural properties

In Fig. 8, the density profiles of water oxygen and water hydrogen atoms as a function of z (perpendicular to the lignite surface) are shown. The atomic oxygen density profile has a first peak at 13.37 Å, which clearly means the formation of one hydration layer of water molecules. In addition, a second peak was detected at 15.47 Å. For the atomic hydrogen density profile, a distinct peak is located at 14.07 Å, and a second peak appears at approximately 16.03 Å. At distances larger than about 20 Å, the hydrogen and oxygen density profiles become smooth, indicating bulk-like behavior. These profiles suggest that the lignite surface properties affect the structural and dynamic characteristics of the interfacial water molecules. The water molecules at the lignite/water interface are much more ordered than those far from the lignite surface.

The structural organization of water in the lignite matrix can be described by lignite–water radial distribution functions (RDF) representing the relative probability of finding any water molecule with its oxygen atom at a distance r from any oxygen atom of the lignite model. As shown in Fig. 9, there is a peak in the RDF at 2.65 Å that results from the strong hydrogen-bond interactions created between the interfacial water molecules and the oxygen-containing functional groups on the lignite surface (Zhang, 2011). This result confirms that the oxygen-containing functional groups are responsible for the adsorption of water molecules. In addition, according to the $O_{lignite}$ -O_{water} RDF, the first hydration shell is within a 3.9 Å cutoff.

3.4. MD simulations: dynamic properties of water molecules around oxygen functional groups

To better understand the dynamic properties of the water molecules in the vicinity of the different oxygen-containing functional groups on the lignite model surface, the MSD and the local self-diffusion coefficient of the water molecules in the above defined first hydration shell were computed. Fig. 10 shows the MSDs of the water molecules near carboxyl, carbonyl, and hydroxyl groups, respectively, and suggests that the mobility of the water molecules is affected by the type of oxygen-containing functional groups on the lignite surface.

The local self-diffusion coefficients of the water molecules in the first hydration shell of oxygen-containing functional groups were computed using the above mentioned 3.9 Å cutoff. The self-diffusion coefficients of the water molecules in the vicinity of carboxyl, carbonyl, and hydroxyl groups were calculated to be 5.58×10^{-5} cm^2/s, 7.37×10^{-5} cm^2/s, and 6.05×10^{-5} cm^2/s, respectively.

In order to certify the aforementioned distinct water dynamics around the different oxygen-containing functional groups (hydroxyl, carbonyl, and carboxyl), MD simulations containing only one of these functional groups on a graphite surface solvated by 250 water molecules were carried out and compared. The modified graphite models are shown in Fig. 11. The MSD plots are displayed in Fig. 12. The calculated water self-diffusion coefficients around carboxyl, carbonyl, and hydroxyl groups are 3.70×10^{-5} cm^2/s, 4.79×10^{-5} cm^2/s, and 4.35×10^{-5} cm^2/s, respectively.

It was found that water mobility in the proximity of carboxylic groups appears to be retarded. This can be attributed to the formation of strong hydrogen bond interactions between the carboxyl moieties and the water molecules. These results confirm that, in comparison with the other functional groups investigated, carboxyl groups have the strongest hydration ability and are the preferential adsorption sites. The hydration ability of the different oxygen-containing functional groups follows the order carboxyl > hydroxyl > carbonyl. These results are consistent with previous studies (Nishino, 2001).
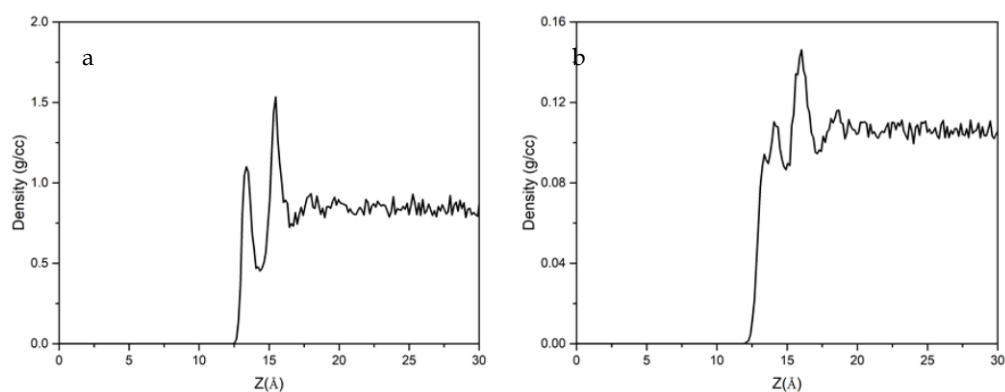

Fig. 8. Oxygen (a) and hydrogen (b) atom density profiles along the z axis
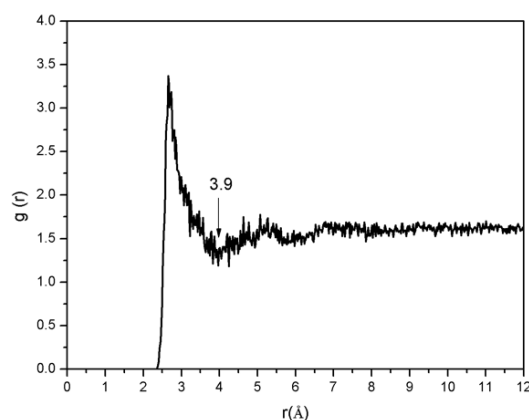

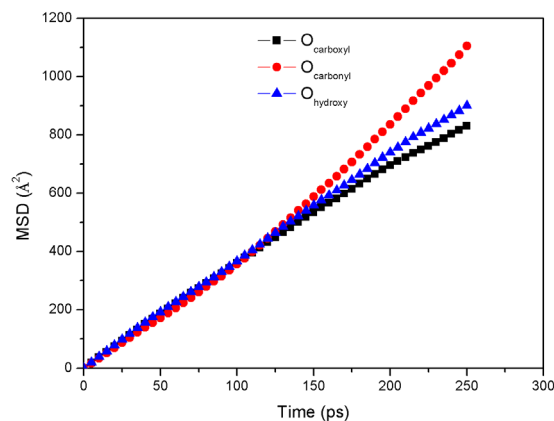Fig. 9. Radial distribution function g(r) of the O$_{lignite}$-O$_{water}$ pair

Fig. 10. MSDs of the water molecules around carboxyl, carbonyl, and hydroxyl, respectively; self-diffusion coefficients were calculated and assigned to their corresponding curves
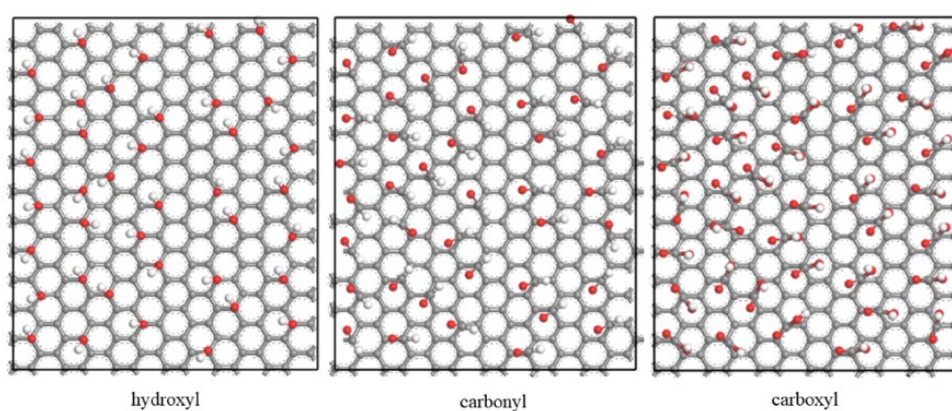

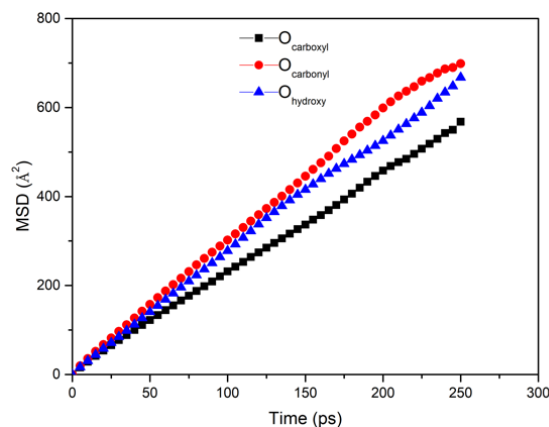Fig. 11. Top view of the modified graphite models

Fig. 12. MSDs of water molecules near the graphite surfaces containing carboxyl, carbonyl, or hydroxyl groups

4. Conclusions

The effects of oxygen-containing functional groups on the lignite surface on the structure and dynamic properties of the interfacial water molecules were obtained using molecular dynamics simulations. Because of its complex composition and structure, a graphite surface containing hydroxyl, carboxyl, and carbonyl groups was employed to represent the surface model of lignite. According to the XPS results, the composing proportion of hydroxyl, carbonyl, and carboxyl is 21:13:6. The calculated oxygen and hydrogen atomic density profiles show the formation of two hydration layers. In addition, the atomic density profiles indicate that the lignite surface properties affect the structural and dynamic

characteristics of the interfacial water molecules. The water molecules at the lignite/water interface are much more ordered than those far from the lignite surface. The results of the radial distribution functions, mean square displacements, and local self-diffusion coefficients for the water molecules in the vicinity of the three oxygen-containing functional groups confirm that carboxyl groups are the preferential adsorption sites.

Acknowledgments

References

ALLARDICE, D., EVANS, D., 1971. *The-brown coal/water system: Part 2. Water sorption isotherms on bed-moist Yallourn brown coal.* Fuel. 50, **236**-253.

ARGYRIS, D., COLE, D. R., STRIOLO, A., 2009. *Hydration structure on crystalline silica substrates.* Langmuir. 25, **8025**-8035.

ARGYRIS, D., TUMMALA, N. R., STRIOLO, A., COLE, D. R., 2008. *Molecular Structure and dynamics in thin water films at the silica and graphite surfaces.* J. Phys. Chem. C. 112, **13587**-13599.

BERENDSEN, H., GRIGERA, J., STRAATSMA, T., 1987. *The missing term in effective pair potentials.* J. Phys. Chem. 91, **6269**-6271.

BHATTACHARYYA, K., 1971. *The role of sorption of water vapour in the spontaneous heating of coal.* Fuel. 50, **367**-380.

BUNTE, S. W., SUN, H., 2000. *Molecular modeling of energetic materials: The parameterization and validation of nitrate esters in the COMPASS force field.* J. Phys. Chem. B. 104, **2477**-2489.

GAO, Y.S., GAO, Z.Y., SUN, W., YIN, Z.G., WANG, J.J., HU Y.H.,2018. *Adsorption of a novel reagent scheme on scheelite and calcite causing an effective flotation separation.* J. Colloid Interface Sci., 512, 39-46.

GAO, Z.Y., LI, C.W., SUN, W., HU, Y.H., 2017. *Anisotropic surface properties of calcite: A consideration of surface broke n bonds.* Colloid. Surface. A., 520, 53-61.

GAO, Y.S., GAO, Z.Y., SUN, W., HU, Y.H., 2016 a. *Selective flotation of scheelite from calcite: A novel reagent scheme*, International Journal of Mineral Processing, 154,10-15.

GAO, Z.Y., GAO, Y.S., ZHU, Y.Y., HU, Y.H., SUN, W., 2016 b. *Selective flotation of calcite from fluorite: a novel reagent schedule.* Minerals, 6 (4), 114.

HE, M., ZHANG, W., CAO, X., YOU, X., LI, L., 2018. *Adsorption behavior of surfactant on lignite surface: A comparative experimental and molecular dynamics simulation study.* Int. J. Mol. Sci. 19, **437**.

LARSEN, J. W., BASKAR, A. J., 1987. *Hydrogen bonds from a subbituminous coal to sorbed solvents. An infrared study.* Energ. Fuel. 1, **230**-232.

LI, C., GAO Z., 2017. *Effect of grinding media on the surface property and flotation behavior of scheelite particles.* Powder Technol, 322, 386-392.

LIU, H. T., ISHIZUKA, T., TAKANOHASHI, T., IINO, M., 1993. *Effect of TCNE addition on the extraction of coals and solubility of coal extracts.* Energ. Fuel. 7, **1108**-1111.

LIU, W., XU, S., ZHAO, X., YUAN, G., MIMURA, H., 2013. *Adsorption mechanism of chlorides on carbon nanotubes based on first-principles calculations.* Chem. Phys. Lett. 580, **94**-98.

LIU, X., LIU, S., FAN, M., ZHANG, L., 2017. *Decrease of hydrophilicity of lignite using CTAB: Effects of adsorption differences of surfactant onto mineral composition and functional groups.* Fuel. 197, **474**-481.

LYU, X., YOU, X., HE, M., ZHANG, W., WEI, H., LI, L., HE, Q., 2018. *Adsorption and molecular dynamics simulations of nonionic surfactant on the low rank coal surface.* Fuel. 211, **529**-534.

MCQUAID, M. J., SUN, H., RIGBY, D., 2004. *Development and validation of COMPASS force field parameters for molecules with aliphatic azide chains.* J. Comput. Chem. 25, **61**-71.

MIYAKE, M., STOCK, L. M., 1988. *Coal solubilization. Factors governing successful solubilization through C-alkylation.* Energ. Fuel. 2, **815**-818.

MUKHERJEE, S., BORTHAKUR, P. C., 2004. *Demineralization of subbituminous high sulphur coal using mineral acids.* Fuel Process. Technol. 85, **157**-164.

NISHINO, J., 2001. *Adsorption of water vapor and carbon dioxide at carboxylic functional groups on the surface of coal.* Fuel. 80, **757**-764.

NORINAGA, K., KUMAGAI, H., HAYASHI, J.-I., CHIBA, T., 1998. *Classification of water sorbed in coal on the basis of congelation characteristics.* Energ. Fuel. 12**,** 574-579.

OSMAN, H., JANGAM, S., LEASE, J., MUJUMDAR, A. S., 2011. *Drying of low-rank coal (LRC) – a review of recent patents and innovations.* Drying Technol. 29**,** 1763-1783.

PIETRZAK, R., WACHOWSKA, H., 2006. *The influence of oxidation with HNO_3 on the surface composition of high-sulphur coals: XPS study.* Fuel Process. Technol. 87**,** 1021-1029.

QUINGA, E. M., LARSEN, J. W., 1987. *Noncovalent interactions in high-rank coals.* Energ. Fuel. 1**,** 300-304.

SHIH, C. J., LIN, S., SHARMA, R., STRANO, M. S., BLANKSCHTEIN, D., 2012. *Understanding the pH-dependent behavior of graphene oxide aqueous solutions: A comparative experimental and molecular dynamics simulation study.* Langmuir. 28**,** 235-241.

SUN, H., REN, P., FRIED, J. R., 1998. *The COMPASS force field: parameterization and validation for phosphazenes.* Comput. Theor. Polym. Sci. 8**,** 229-246.

TAO, C., FENG, H., ZHOU, J., LV, L., LU, X., 2009. *Molecular simulation of oxygen adsorption and diffusion in polypropylene.* Acta Phys-Chim. Sin. 25**,** 1373-1378.

TIAN, B., QIAO, Y. Y., TIAN, Y. Y., LIU, Q., 2016a. *Investigation on the effect of particle size and heating rate on pyrolysis characteristics of a bituminous coal by TG–FTIR.* J. Anal. Appl. Pyrolysis. 121**,** 376-386.

TIAN, B., QIAO, Y. Y., TIAN, Y. Y., XIE, K. C., LIU, Q., ZHOU, H. F., 2016b. *FTIR study on structural changes of different–rank coals caused by single/multiple extraction with cyclohexanone and NMP/CS_2 mixed solvent.* Fuel Process. Technol. 154**,** 210-218.

TIAN, M., GAO, Z., HAN, H., SUN, W., HU, Y., 2017. *Improved flotation separation of cassiterite from calcite using a mixture of lead (II) ion / benzohydroxamic acid as collector and carboxymethyl cellulose as depressant.* Miner Eng, 113, 68-70.

TUMMALA, N. R., SHI, L., STRIOLO, A., 2011. *Molecular dynamics simulations of surfactants at the silica–water interface: Anionic vs nonionic headgroups.* J. Colloid Interface Sci. 362**,** 135-143.

VU, T., CHAFFEE, A., YAROVSKY, I., 2002. *Investigation of lignin-water interactions by molecular simulation.* Mol. Simulat. 28**,** 981-991.

WANG J., GAO Z., GAO Y., HU Y., SUN W, 2016. *Flotation separation of scheelite from calcite using mixed cationic/anionic collectors*. Miner Eng, 98, 261-263.

WENDER, I., 2006. *Catalytic synthesis of chemicals from coal.* Catal. Rev. 14**,** 97-129.

WILLSON, W. G., WALSH, D., IRWINC, W., 1997. *Overview of low-rank coal (LRC) drying.* Coal Prep. 18**,** 1-15.

WU, J., LIU, J., YUAN, S., WANG, Z., ZHOU, J., CEN, K., 2016. *Theoretical investigation of noncovalent interactions between low-rank coal and water.* Energ. Fuel. 30**,** 7118-7124.

YANG, J., REN, Y., TIAN, A., SUN, H., 2000. *COMPASS force field for 14 inorganic molecules, He, Ne, Ar, Kr, Xe, H_2, O_2, N_2, NO, CO, CO_2, NO_2, CS_2, and SO_2, in liquid phases.* J. Phys. Chem. B. 104**,** 4951-4957.

YOU, X., HE, M., ZHANG, W., WEI, H., HE, Q., LYU, X., LI, L., 2018. *Molecular dynamics simulations and contact angle of surfactant at the coal–water interface.* Mol. Simulat. 44**,** 722-727.

YOU, X., LI, L., LIU, J., WU, L., HE, M., LYU, X., 2017. *Investigation of particle collection and flotation kinetics within the Jameson cell downcomer.* Powder Technol. 310**,** 221-227.

ZHANG, H., SHI, H., CHEN, J., ZHAO, K., WANG, L., HAO, Y., 2016. *Elemental mercury removal from syngas at high-temperature using activated char pyrolyzed from biomass and lignite.* Korean J. Chem. Eng. 33**,** 3134-3140.

ZHANG, L., LI, B., XIA, Y., LIU, S., 2017. *Wettability modification of Wender lignite by adsorption of dodecyl poly ethoxylated surfactants with different degree of ethoxylation: A molecular dynamics simulation study.* J. Mol. Graph. Model. 76**,** 106-117.

ZHANG, Z., 2011. *Structure and dynamics in brown coal matrix during moisture removal process by molecular dynamics simulation.* Mol. Phys. 109**,** 447-455.

ZHANG, Z., WANG, C., YAN, K., 2015. *Adsorption of collectors on model surface of wiser bituminous coal: a molecular dynamics simulation study.* Miner. Eng. 79**,** 31-39.

ZHOU, G., QIU, H., ZHANG, Q., XU, M., WANG, J., WANG, G., 2016. *Experimental investigation of coal dust wettability based on surface contact angle.* J. Chem-NY. 2016**,** 13-18.

ZHOU, G., XU, C., CHENG, W., ZHANG, Q., NIE, W., 2015. *Effects of oxygen element and oxygen-containing functional groups on surface wettability of coal dust with various metamorphic degrees based on XPS experiment.* J. Anal. Methods Chem. 2015**,** 72-76.